RSC Advances

RSC Advances

www.rsc.org/advances

ROYAL SOCIETY
OF CHEMISTRY

www.rsc.org/advances

Graphical Abstract

The microwave absorption properties of the ultra-thin and crumpled ZnS nets-wrapped walnut-like Ni composites are superior to those of pristine Ni walnuts.
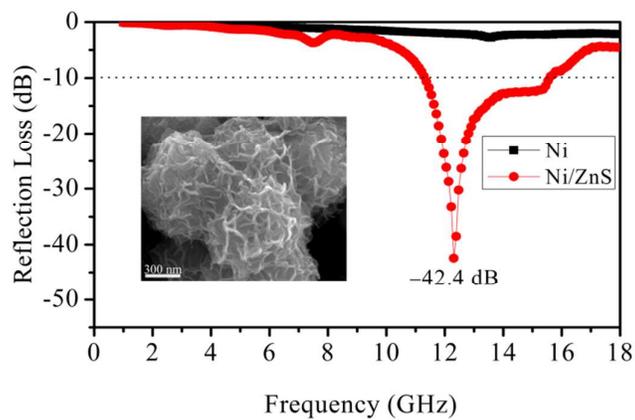
Facile synthesis of crumpled ZnS net–wrapped Ni walnut spheres with enhanced microwave absorption properties

Biao Zhao [a], Gang Shao [a] *, Bingbing Fan [a], Wanyu Zhao [a], Yongqiang Chen [a], Rui Zhang [a, b] *

ABSTRACT: Controllable magnetic-dielectric hybrids with core of walnut-like Ni and shell of ultra-thin and crumpled ZnS nets have been successfully synthesized by a facile two-step approach. The morphology, microstructure and microwave absorption properties of the as-synthesized core-shell Ni/ZnS composites were investigated by scanning electron microscopy, energy dispersive X-ray spectroscopy, X-ray diffraction, transmission electron microscopy and network analyzer. The shapes and microwave absorption
10 properties of Ni/ZnS can be tuned by the hydrothermal temperatures. The core-shell Ni/ZnS composites present significantly enhanced microwave absorption compared with pristine Ni walnuts. When the reaction temperature was 60°C, the reflection loss (RL) could be as low as -42.4 dB at 12.3 GHz. Moreover, the effective bandwidth (RL< -10 dB) can be recorded in the 11.3-15.6 GHz rang with the absorber thickness of only 2.2 mm. The excellent microwave absorption properties were attributed to impedance match, the synergetic effect between the dielectric loss and magnetic loss, interfacial relaxation and conduction loss of unique cross-linked ZnS shells. These
15 results suggest that the as-synthesized crumpled ZnS net–wrapped Ni composites may be an attractive candidate for microwave absorption application.

1. Introduction

With the rapid proliferation of electronic devices and high
20 frequency circuit devices in the gigahertz (GH) range, electromagnetic interference (EMI) pollution has become a vital concern. [1, 2] The EMI pollution can not only affects various commercial and industrial equipment but also threatens the health of living things by breaking down DNA strands, accelerating
25 heart rate, causing cancer, and so on. [3-5] An effective way to deal with these problems is to pursue a new type of material with strong electromagnetic wave absorbing properties. The main goal of this absorber is to achieve the attenuation of electromagnetic energy through its dielectric loss or magnetic loss, and could be
30 used to minimize the electromagnetic reflection. [6, 7] Microwave absorbing materials are currently needed to have the features of strong absorption, wide waveband, light-weight, thin-thickness, and simple operation. [8, 9]

The microwave absorption performance can be determined by
35 the complex permittivity/permeability, EM impedance match and the microstructures. [10] Among the microwave absorber, metallic magnetic Ni-based materials with high permeability as well as low cost have been extensively investigated, [11-14] which should be expected to avoid the eddy current effect. It stimulates scientists
40 to prepare core-shell structured microwave absorption absorbers,

such as Fe_3O_4/graphene and carbon nanocoils coated with Fe_3O_4 or Ni by atomic layer deposition, [15,16] Fe_3O_4@ZnO nanohybrid, [17] CuO/Cu_2O-coated Ni nanocapsules, [18] Ni/polyaniline, [19] carbon-coated nickel, [20] Ni@Ni_2O_3 particles, [21] carbon-coated iron, [22]
45 Fe_3O_4 microspheres/Polyaniline, [23] and Fe_3O_4/carbon nanorods, [24] which exhibit better microwave absorption performance than the pure core or shell materials. These kind of absorber materials, which combine with the magnetic loss of cores and dielectric loss of shells as well as special core-shell structures, give rise to the
50 enhanced microwave absorption capabilities. Therefore, preparation of magnetic–dielectric composite with core-shell structure is beneficial for excellent microwave absorption abilities.

ZnS is a wide band-gap semiconductor with a band-gap
55 energy (Eg) of 3.6 eV. It has been used widely in displays, sensors, and lasers for many years. [25, 26] To the best of our knowledge, there are scarce literatures about the microwave absorption properties of ZnS-based were presented. In our earlier report, [27] wall-like ZnS-coated Ni composites were successfully
60 prepared. Compared with pure Ni microspheres with the diameter of 0.9 μm, Ni/ZnS composites exhibit the enhanced microwave absorption properties. However, the size of Ni spheres were too

large and the effect of morphologies on the microwave absorption properties of Ni/ZnS composites were not investigated.

In this present work, the walnut-like Ni particles with the average size of 500 nm and crumpled ZnS nets-wrapped Ni walnuts have been successfully synthesized. The morphologies and microwave absorption properties of core-shell Ni/ZnS were determined by the hydrothermal temperature. The ultra-thin and crumpled ZnS-wrapped Ni walnuts prepared at 60°C show the best microwave absorption capability. The optimal reflection loss is -42.4 dB at 12.3 GHz. These results suggest that we have paved a new way to fabricate novel microwave absorbing materials and extend the application of semiconductor ZnS materials.

2.   Experimental section

2.1. Materials. All the chemical reagents were of analytical grade and used without any further purification. Nickel chloride hexahydrate ($NiCl_2 \cdot 6H_2O$), glycerol, trisodium citrate dihydrate, $NH_3 \cdot H_2O$ and sodium acetate were supplied by Xilong Chemical Reagent Co. Ltd. (Guangdong, China). $Zn(CH_3COO)_2 \cdot 2H_2O$, and $NaH_2PO_2 \cdot H_2O$ were provided by Kemiou Chemical Reagent Co. Ltd. (Tianjin, China). $Na_2S \cdot 9H_2O$ was purchased from Fengchuan Chemical Reagent Technologies Co. Ltd. (Tianjin, China). The thin and crumpled ZnS nanonet–wrapped Ni walnut spheres were prepared through a two-stage method.

2.2. Preparation of Ni walnut spheres. In a typical procedure, $NiCl_2 \cdot 6H_2O$ (1.2 g), trisodium citrate dihydrate (0.2 g) and sodium acetate (3.0 g) were dissolved in mixture solution containing 30 mL glycerol and 30 ml distilled water. Then NaOH(1.6 g) was added into the solution. Afterwards, sodium hypophosphite ($NaH_2PO_2 \cdot H_2O$, 3.2 g) was added to the above mixture. Finally, the solution was transferred into a Teflon-lined stainless steel autoclave, which was then sealed and kept in an oven at 140°C for 15 h. The black precipitate was collected and rinsed with distilled water and ethanol, and finally dried in a vacuum oven.

**2.3 Preparation of ZnS nanonet–wrapped Ni walnut spheres.** In a typical experiment, the as-prepared Ni walnut spheres (0.05 g) and $Zn(CH_3COO)_2 \cdot 2H_2O$ (0.45 g) were dispersed in a mixture of ethanol (30 mL) and distilled water (30 mL). Then, $Na_2S \cdot 9H_2O$ (0.50 g) and ammonia solution (4 mL) were introduced into the above mixture solution with intensely stirring over 20 min. Then the mixture was transferred into a Teflon-lined stainless steel autoclave, and maintained at 60 °C for 15 h. When cooled to room temperature, the final precipitates were washed with distilled water and absolute ethanol. In order to investigate the effect of temperature on the morphologies and microwave absorption properties of the Ni/ZnS composites. Three temperatures (40°C, 60°C, 80°C) were conducted in this experiment. The corresponding products were denoted as S-1, S-2 and S-3 samples, respectively.

2.4. Characterization. The crystal structure of the as-obtained samples were analyzed by X-ray diffraction (XRD, XD-3, Beijing Purkinje General Instrument Co. Ltd.).   The morphologies of samples were observed by field emission scanning electron microscopy (FESEM, JEOL JSM-7001F) and transmission electron microscope (TEM, JEOL JEM-2010). The element composition was carried out by an energy dispersive X-ray spectroscopy (EDS, Oxford Instruments) equipped with FESEM. To probe the microwave absorption properties of Ni walnut spheres and core-shell Ni/ZnS composites, the electromagnetic parameters of the Ni walnut spheres and Ni/ZnS composites were measured using a vector networker (Agilent, N5244A) in the frequency of 1-18 GHz. Paraffin composite samples containing 40 wt% as-obtained products were pressed into toroidal-shape (Φ_{out}: 7.00 mm, Φ_{inner}: 3.04 mm) for microwave measurement. The paraffin wax was employed as the binder, which is transparent for electromagnetic wave.

3. Results and discussion

Fig.1 presents the X-ray diffraction (XRD) patterns of as-prepared Ni walnut spheres and core-shell Ni/ZnS composites. As shown in Fig.1a, all the diffraction peaks are perfectly indexed to the face-centered cubic phase of Ni (JCPDS no. 04-0850). After wrapped by ZnS nanonet, the diffraction peaks corresponding to both Ni and ZnS (JCPDS Card No. 05-0566)

can be clearly seen. No other phases are observed except for the Ni and ZnS phases. According to the Fig.1, it can be inferred that the as-synthesized core/shell structured composites are comprised of crystalline Ni and ZnS.
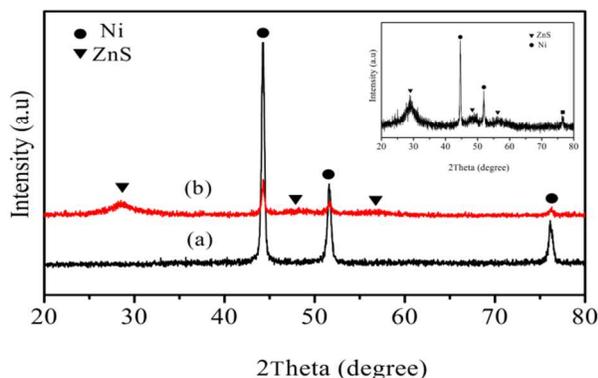

Fig. 1 XRD patterns of (a) walnut-like Ni particle and (b) core-shell Ni/ZnS composites. Inset is the XRD profile of Ni/ZnS composite.

The morphologies of Ni particles and Ni/ZnS composites were investigated using the FESEM, as shown in Fig.2. According to the Fig.2a, the as-synthesized Ni shows the narrow size distribution of walnut-like shapes with the average diameter of 500 nm. In addition, the synthesized Ni products appear to possess superior dispersibility. Fig.2(b-d) exhibit the different magnification images of Ni/ZnS composites. From the panoramic images of Ni/ZnS (Fig.2b), it can be found that the surfaces of composites were comprised of ZnS nano-nets compared with pristine walnut-like Ni particles. Fig.2(c,d) show the amplified image of Ni/ZnS composite microspheres, which indicate the existence of ultra-thin and crumpled structured ZnS nets on the surfaces of Ni particles. The peanut-like Ni particles were densely wrapped by ultra-thin and crumpled ZnS nets to form core-shell structures. The unique crumpled and rippled structured ZnS nano-nets might give rise to multi-reflection when the microwaves are incident on the Ni/ ZnS composites, which is beneficial for the microwave attenuation.
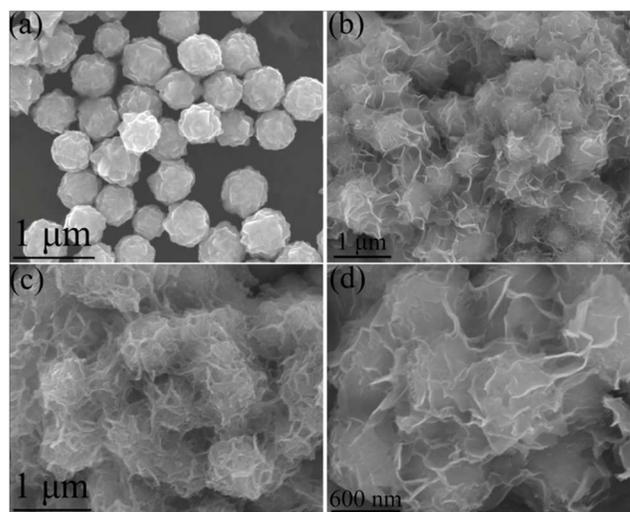
Fig. 2 (a) FESEM image of Ni walnuts and (b-d) different magnification FESEM images of ZnS nanonet-wrapped Ni composites.
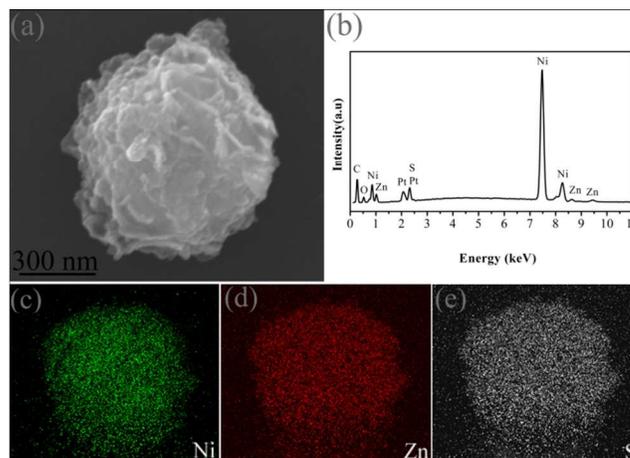
Fig. 3 (a) FESEM image of an individual Ni/ZnS composites, (b) EDS pattern of Ni/ZnS composite and (c-e) corresponding elemental mappings of Ni, Zn and S.

In order to get more information of core-shell structured Ni/ZnS composites, the morphology of an individual Ni/ZnS composite microsphere and energy-dispersive X-ray spectroscopy (EDS) were performed (Fig.3a,b). The EDS result shown in Fig.3b indicates that the obtained composites are composed of Ni, Zn and S elements. The carbon and oxygen elements are also appeared in the EDS spectrum, which possibly comes from the carbon conductive tape to support the samples during the test and the oxygen residual or oxide in the composite, respectively. To

illustrate the spatial distribution of Ni, Zn and S elements in the composite spheres, elemental mapping was performed on a representative Ni@ZnS core–shell composite (Fig. 3c-e) under FESEM observation. The elemental mapping results demonstrate
5 the generally uniform distribution of Ni/ZnS composite microspheres (Fig.3c-e)
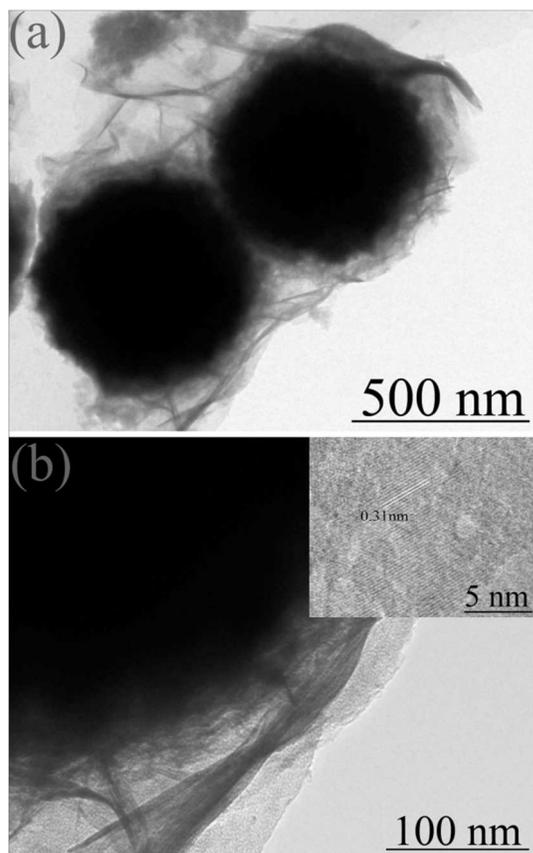
**Fig. 4** TEM images of crumpled ZnS net-wrapped Ni walnut sphere composite with different magnifications. Inset of (b)
10 shows the HRTEM of ZnS shell.

Furthermore, to further validate the core-shell structure of Ni/ZnS composites, the TEM images of the attained composites are applied to characterize the morphology in detail (Fig.4). The thin ZnS shells have a crumpled and rippled structure. The
15 interfaces between Ni and ZnS could be clearly observed. Moreover, the Ni/ZnS composites show a typical cross-linked framework structure. The HRTEM image (inset of Fig.4b) of the ultra-thin shell region of core-shell structure shows that the fringe spacing is about 0.31 nm, corresponding to the (111) crystal
20 planes of the zinc blende ZnS, which is in accordance with XRD result. From the SEM and TEM images, it can be concluded that

the walnut-like Ni powders are wrapped by thin and crumpled ZnS nets to form core-shell structure.
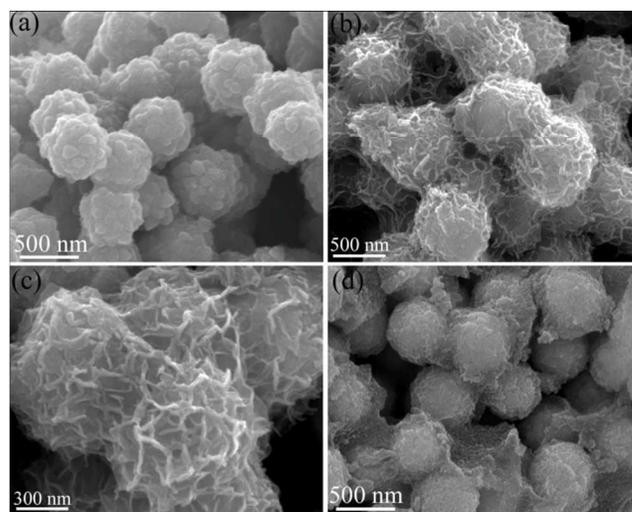
25 **Fig. 5** FESEM images of hierarchical Ni/ZnS core-shell composites prepared at different temperature: (a) S-1 (40 °C); (b, c) S-2 (60 °C); (d) S-3 (80 °C).

Fig.5 shows the morphologies of the Ni/ZnS composites prepared at various hydrothermal temperatures. It is worth noting
30 that the surfaces of all samples turns coarser compared with the pure Ni walnuts, which could be attributed to the successful coating of the ZnS on the primary Ni surfaces. Furthermore, the shapes of ZnS shells could be controlled by the reaction temperatures. At low temperature (40 °C, S-1), the walnut-like Ni
35 submicrospheres were coated by relatively loose ZnS nanoparticles (Fig.5a). When the hydrothermal temperature was increased to 60 °C (S-2), ultra-thin and crumpled structured ZnS nets were produced on the surfaces of Ni walnut spheres (Fig.5b,c). The unique cross-linked framework structures
40 between Ni particles and thin ZnS nets endow the composite with the features of high surface area and allow more microwave enter, which is favorable to the microwave energy attenuation. When the reaction temperature is further increased to 80 °C (S-3), the densely ZnS particles are deposited on the surfaces of Ni
45 powders. Meanwhile, the thickness of ZnS shells was increased in comparison with S-1 and S-2 samples. The dense and thick shells might damage the electromagnetic impedance, which hamper the microwave enter in the absorbing materials. From the

above results, it can be deduced that the structures of ZnS shells can be effectively determined by an appropriate hydrothermal
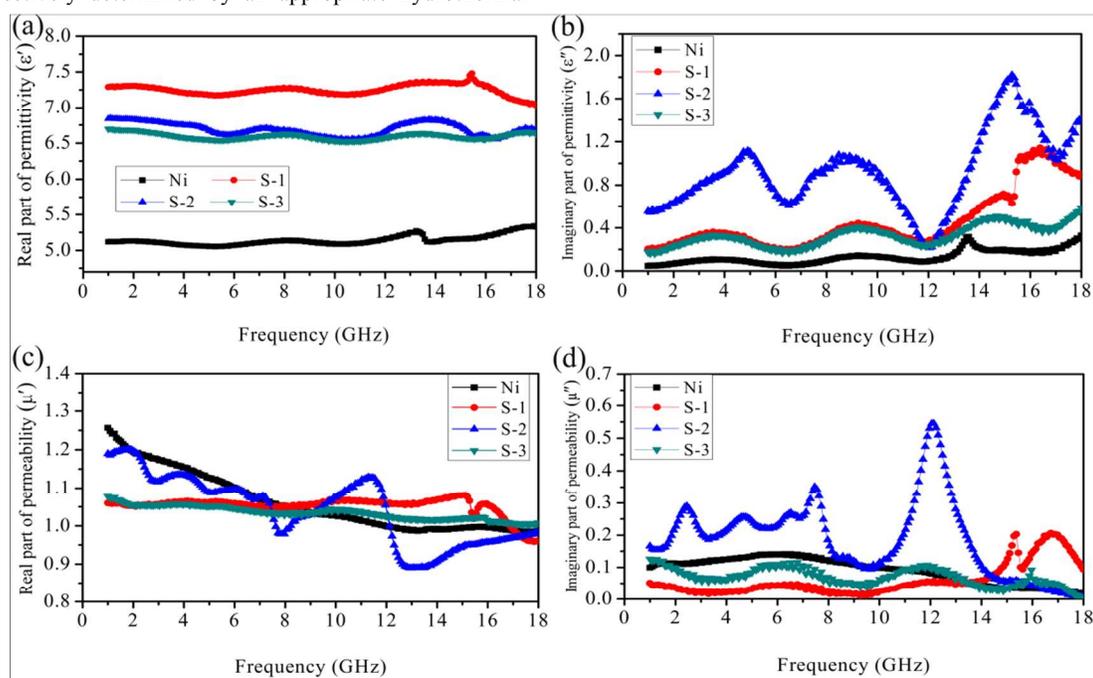
temperature.

Fig. 6 Frequency dependence of the (a) real and (b) imaginary parts of complex permittivity, and the (c) real and (d) imaginary parts of complex permeability for the Ni and three Ni/ZnS samples.

Microwave absorption properties of a absorber are highly associated with its complex permittivity and complex permeability. Fig. 6 shows the complex relative permittivity ($\varepsilon_r = \varepsilon' - j\varepsilon''$, ε' and ε'' are the real and imaginary part of complex permittivity) and permeability ($\mu_r = \mu' - j\mu''$, μ' and μ'' are the real and imaginary part of complex permeability) of walnut-like Ni particles and core-shell Ni/ZnS composites. It is well known that the real part of complex permittivity (ε') is relative to the polarization and imaginary part (ε'') represents the dielectric loss capability of absorbing materials.[28, 29] As shown in Fig.6a, it can be found that the ε' values of Ni/ZnS composites were higher than those of Ni walnuts, which implies more polarization for the Ni/ZnS composites. It can be attributed to the more interfaces of unique core-shell structures. Notably, the ε' of S-1 sample is higher than that of S-2 and S-3 samples. However, according to the previous reports,[30-32] high real part of complex permittivity might lead to impedance mismatch, which is harmful to the microwave absorption properties. It can be deduced that an

appropriate ε' values is necessary for the better microwave attenuation. Fig.6b shows the imaginary parts (ε'') of walnut-like Ni particles and core-shell Ni/ZnS composites. Interestingly, one can see that S-2 sample exhibits the highest ε'' values among the four samples, which means the highest dielectric loss for the S-2 sample. It is worthy to notice that the four samples present multi-peaks on the ε'' values, suggesting a resonance behavior, which is expected when the composite is highly conductive and skin effect becomes significant.[33] Moreover, especially for the Ni/ZnS composites, these phenomena are also called the nonlinear resonant behaviors, [34] which originates mainly from the cooperative consequence of the Ni cores, the core/shell interfaces and the dielectric ZnS shells. [35, 36] According to the free electron theory, [37, 38] $\varepsilon'' \approx 1/\pi\varepsilon_0\rho f$, where ρ is the resistivity. The electric resistivity of the Ni samples is higher than that of the ZnS@Ni samples. The high electric resistivity of the Ni samples was assigned to the low filler ration (40 wt%) and high dispersion in the paraffin composites. However, for the Ni/ZnS composites,

especially for the S-2 samples, the ultra-thin and crumpled cross-linked ZnS nets can connect with each other and a continuous microcurrent gradually forms, which will give rise to low electric resistivity and cause electric and conduction loss.[39]

5 The real part (μ') and imaginary part (μ'') of the relative complex permeability are plotted as a function of frequency in Fig. 6c–d. The μ' of Ni particles and core-shell Ni/ZnS composites gradually decreased with increasing frequency (Fig.6c). However, the μ' values of S-2 sample show large 10 fluctuation, which was due to the unique crumpled ZnS nets-wrapped Ni walnut composites. Imaginary parts (μ'') stand for the magnetic loss of the microwave dissipated capability. From the Fig.6d, it can be seen that S-2 sample exhibits the highest μ'' values, which indicates the highest magnetic loss among the four 15 paraffin-composites. Furthermore, for the Ni/ZnS composites, the μ'' values show the multi-peaks, which suggest the resonance behaviors. Generally, the resonance can be assigned to natural resonance in the low frequency,[40] while other resonances could be attributed to exchange resonances in the high frequency. [41, 42]
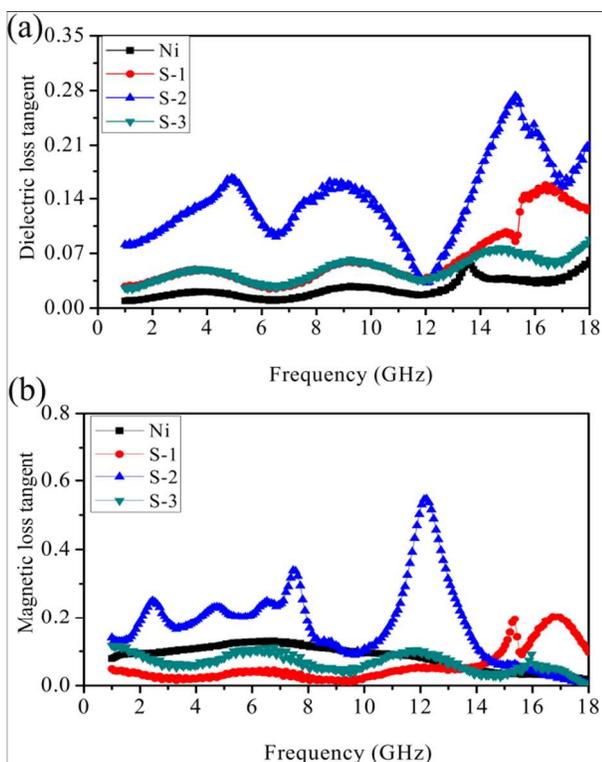

Fig. 7 (a) The dielectric loss factor and (b) magnetic loss factor of Ni particles and Ni/ZnS–paraffin wax samples versus frequency.

The dielectric loss tangent (tan $\delta_\varepsilon = \varepsilon''/\varepsilon'$) and magnetic loss 25 tangent (tan $\delta_\mu = \mu''/\mu'$) are universally used to evaluate electromagnetic loss capacity.[43] The higher values of tan δ_ε and tan δ_μ indicate the greater dielectric loss and magnetic loss. The dielectric loss factor (tan $\delta_\varepsilon = \varepsilon''/\varepsilon'$) and magnetic loss factor (tan $\delta_\mu = \mu''/\mu'$) of the Ni particles and Ni/ZnS composites are 30 presented in Fig. 7. S-2 sample exhibits the highest dielectric loss and magnetic loss among the four samples, which might indicates the outstanding capability of microwave absorption. It is noteworthy that both the dielectric loss and magnetic loss exhibit multi-peaks from the Fig.7. Moreover, for the S-2 sample, the 35 dielectric loss shows the maximum values while magnetic loss exhibits minimum values. Such complementarities between the dielectric loss and the magnetic loss endows the S-2 with the best microwave absorption ability.
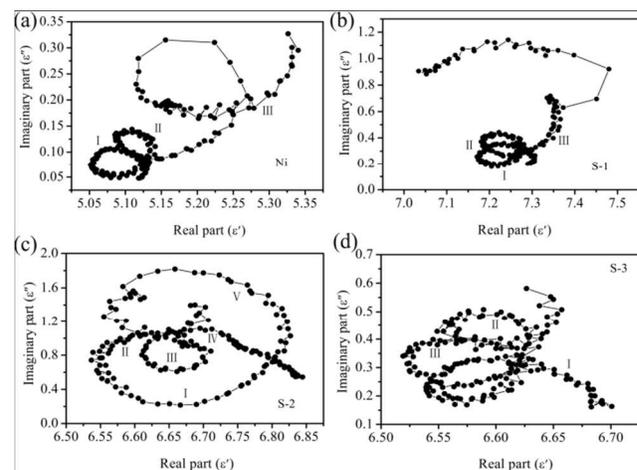
40 **Fig. 8** Typical Cole-Cole semicircles (ε'' versus ε') for Ni particles and Ni/ZnS composites in the frequency range of 1-18 GHz.

To further understand the mechanism of dielectric loss in the absorbing materials, the Debye dipolar relaxation was accounted 45 for the dielectric loss. According to the Debye dipolar relaxation, the relative complex permittivity can be expressed by the following equation: [44-48]

$$\varepsilon_r = \varepsilon_\infty + \frac{\varepsilon_s - \varepsilon_\infty}{1 + j2\pi f\tau} = \varepsilon' - j\varepsilon'' \qquad (1)$$

where $\varepsilon_s, \varepsilon_\infty, f, \tau$ are the static permittivity, relative dielectric permittivity at the high-frequency limit, frequency and polarization relaxation time, respectively. Thus, ε' and ε'' can be described by

$$\varepsilon' = \varepsilon_\infty + \frac{\varepsilon_s - \varepsilon_\infty}{1 + (2\pi f)^2 \tau^2} \qquad (2)$$

$$\varepsilon'' = \frac{2\pi f\tau(\varepsilon_s - \varepsilon_\infty)}{1 + (2\pi f)^2 \tau^2} \qquad (3)$$

based on eqn (2) and (3), the relationship between ε' and ε'' can be deduced

$$\left(\frac{\varepsilon' - \varepsilon_\infty}{2}\right)^2 + (\varepsilon'')^2 = \left(\frac{\varepsilon_s - \varepsilon_\infty}{2}\right)^2 \qquad (4)$$

Thus, the plot of ε' versus ε'' would be a single semicircle, generally denoted as the Cole–Cole semicircle. [49] Each semicircle corresponds to one Debye relaxation process. Fig. 8 shows the curve of ε' as function of ε'' for the paraffin matrix composite containing Ni particle and core/shell structured Ni/ZnS composites. Five semicircles were found in the curves of S-2 sample, indicating the contribution of the Debye relaxation process to the enhanced dielectric properties. However, the Cole–Cole semicircles are distorted, indicating that except for the Debye relaxation, other mechanisms, such as Maxwell–Wagner relaxation [50] and electron polarization also exist in ultra-thin and crumpled ZnS-wrapped Ni paraffin-composite. The former behavior appears in heterogeneous media owing to charges generated at the surfaces between Ni and ZnS. Due to the connective conductor path of cross-linked Ni/ZnS composites, the microcurrent could be produced, which induce electron polarization.
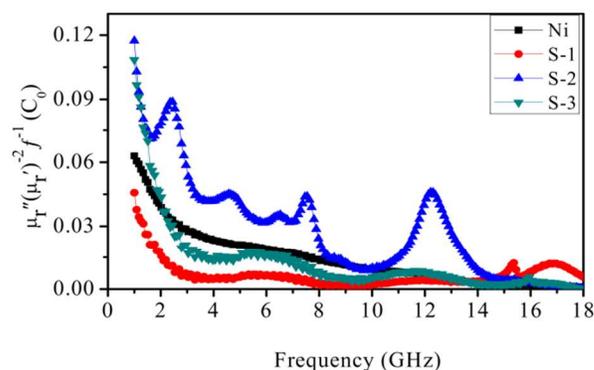

Fig. 9 The value C_0 ($\mu''(\mu')^{-2} f^{-1}$) of Ni particles and Ni/ZnS composite as a function of frequency.

Generally speaking, the magnetic loss of absorbing materials originates from hysteresis loss, domain wall displacement loss, eddy current loss, natural and exchange resonance. In current case, the hysteresis loss is commonly negligible in weak applied field. [51] The domain wall displacement loss often occurs in the MHz range rather than GHz, so the domain wall resonance can also be excluded. [52] The eddy current loss is correlated to the diameter (d) and the electric conductivity (σ), which can be described as: [53, 54] $\mu'' \approx 2\pi\mu_\circ (\mu')^2 \sigma d^2 f / 3$. In which f is the applied frequency, μ_0 is the vacuum permeability. From the above equation, if magnetic loss only originates from eddy current loss, the values of C_0 ($C_0 = \mu''(\mu')^{-2} f^{-1} = 2\pi\mu_0 \sigma d^2 / 3$) should be constant as the frequency is varied. In Ni and Ni/ZnS composite, the value of C_0 decrease gradually with increasing frequency in the whole range of 1–18 GHz (Fig. 9). Thus, the eddy-current loss can be precluded. Therefore, microwave magnetic loss is attributed to the natural resonance and the exchange resonance. Moreover, it is commonly suggested that the natural resonance should occur at lower frequency than the exchange resonance. [55]
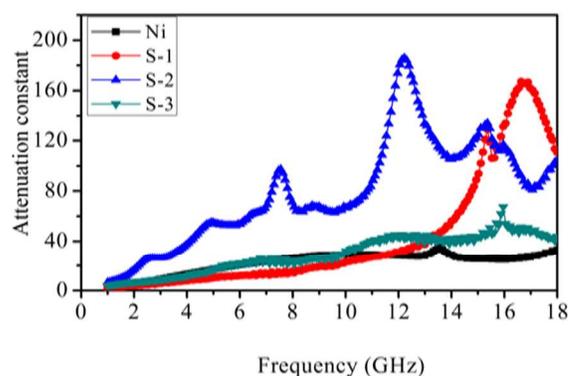
Fig.10 Attenuation constant of Ni particles and Ni/ZnS–paraffin composites versus frequency.

To obtain absorbing materials with excellent microwave absorption capabilities, there are two key problems to be considered. One is the impedance match between the material and free space, [56] which needs the permittivity is close to permeability. The other one is the EM attenuation in the interior absorber. The attenuation constant α determines the attenuation properties of materials. Based on transmission line theory and EM-wave propagation constant, the α can be expressed : [57-59]

$$\alpha = \frac{\sqrt{2}\pi f}{c} \times \sqrt{\left(\mu''\varepsilon'' - \mu'\varepsilon'\right) + \sqrt{\left(\mu''\varepsilon'' - \mu'\varepsilon'\right)^2 + \left(\mu'\varepsilon'' + \mu''\varepsilon'\right)^2}} \quad (5)$$

where f is the frequency of the EM-wave and c is the velocity of light. As shown in Fig.10, the dependence of α on frequency shows that S-2 sample holds the maximum α value among the four samples in most of the tested frequency range,. Therefore, it can be speculated that the S-2 sample (crumpled ZnS net-wrapped Ni) may exhibit better EM-absorption properties than those of Ni particles and other Ni/ZnS samples.
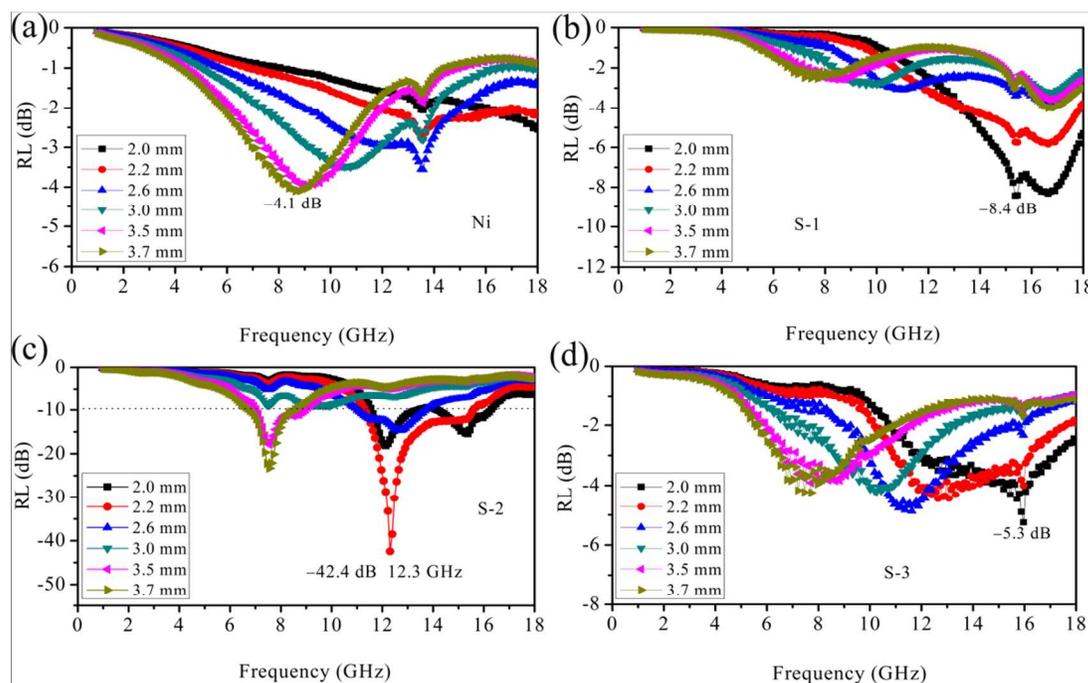
Fig. 11 The reflection losses of (a) Ni particles, (b) S-1, (c) S-2 and (d) S-3 samples with various thicknesses.

To disclose the microwave absorption capability, commonly denoted by the reflection loss (RL), could be simulated on the basis of the relative permeability and permittivity for a given frequency and absorber thickness, by means of the following equations: [3, 60, 51]

$$RL = 20\log\left|\left(Z_{in} - Z_0\right)/\left(Z_{in} + Z_0\right)\right| \quad (6)$$

$$Z_{in} = Z_0\sqrt{\frac{\mu_r}{\varepsilon_r}}\tanh\left(j\frac{2\pi f d\sqrt{\mu_r\varepsilon_r}}{c}\right) \quad (7)$$

where Z_0 is the impedance of free space, Z_{in} is the input characteristic impedance, f is the frequency, c is the velocity of light, and d is the thickness of the composites. Fig.11 shows the calculated theoretical walnut-like Ni and core-shell Ni/ZnS paraffin composites with 40wt% loadings at various thicknesses in the frequency range of 1–18 GHz. It is worth noting that the core-shell Ni/ZnS composites exhibit the enhanced microwave absorption properties compared with pristine walnut-like Ni particles, which might be attributed to the additional interfacial polarization in the core-shell structures. Among the three Ni/ZnS samples, S-2 sample possesses the best electromagnetic wave absorption ability (Fig.11c). The optimal RL of −42.4 dB was obtained at 12.3 GHz and RL values less than -10 dB (90%

microwave attenuation) were observed in the 11.3-15.6 GHz rang with only absorber thickness of 2.2 mm. Interestingly, with increasing absorber thickness, the position of RL peaks almost remains unchanged without shifting to lower frequency, which [5] has also been reported by our previous work [27] and other' groups.[62] The positions of RL peaks were consistent with the natural and exchange resonances, which means the resonance

affects the maximum microwave absorption. Table 1 shows some Ni-based composites and their corresponding microwave [10] absorption performances in recent literatures.[11-14, 19, 20, 30, 32, 35, 63, 64] According to the comparison, the ultra-thin and crumpled ZnS nets-wrapped Ni walnut spheres core-shell composites are very promising to be used as thin-thickness, and high microwave absorptive materials in a wide frequency range.

[15] **Table 1 Some Ni-based composites for microwave absorption in recent literatures**

Sample	Minimum RL Value (dB)	Optimum Thickness (mm)	Optimum Frequency (GHz)	Frequency range (RL<-10 dB)	Ref.
Octahedral Ni	−40.44	2.5	8.8	7.1–11.2	[11]
Ni fiber	−39.5	3.0	4.8	6.6–8.8	[12]
Urchin-like Ni	−43	2.0	10	8.7–11.5	[14]
Ni chains	−19.9	0.8	17.2	16–18	[13]
Ni/SnO$_2$	−18.6	7.0	14.7	13.8–15.3	[30]
Carbon-coated nickel	−32	2.0	13.0	11.2–15.5	[20]
Al$_2$O$_3$-coated Ni	−30.03	2.0	9.2	87.5-13.3	[32]
Ni/polyaniline	−35	5.0	17.2	4.9–6.1 16.2–18	[19]
Ni/Sn$_6$O$_4$(OH)$_4$	−32.4	5.0	13.2	7.2–8.0 12.7–13.8	[35]
Ni/Polypyrrole	−15.2	2.0	13.0	11–15.4	[63]
Ni/TiO$_2$	−35.4	4.0	17.8	17.0–18.0	[64]
Ni/SiO$_2$	−40.0	1.5	12.6	10.9–14.4	[64]
Crumpled ZnS nets-wrapped Ni	−42.4	2.2	12.3	11.3–15.6	This work

4. Conclusion

In summary, the ultra-thin and crumpled ZnS nets-wrapped Ni walnut spheres core-shell composites have been successfully synthesized by a facile two-step process. The morphologies and [20] microwave absorption properties of Ni/ZnS were determined by the hydrothermal temperature. In comparison with pristine walnut-like Ni particles, the core-shell Ni/ZnS composites exhibit better microwave absorption capabilities. The minimum reflection loss of S-2 sample prepared at 60°C was −42.4 dB at [25] 12.3 GHz. Moreover, the effective bandwidth (RL< -10 dB, 90% microwave attenuation) can be observed in the 11.3-15.6 GHz rang with only absorber thickness of 2.2 mm. The outstanding microwave absorption properties are attributed to good impedance match, high attenuation constant, Debye relaxation [30] and interfacial polarization of core-shell structure. As a result, the

as-synthesized cross-linked ZnS net-wrapped Ni hybrid composites have a wide absorption frequency range, strong absorption ability, thin-thickness, which are very attractive for potential applications in EM-wave absorbing materials.

[35] ## Notes and references

[a] *School of Materials Science and Engineering, Zhengzhou University, Zhengzhou 450001, China*

[b] *Laboratory of Aeronautical Composites, Zhengzhou Institute of Aeronautical Industry Management, Zhengzhou 450046, China*

[40] ** Corresponding Author.*

Dr. Gang Shao

E-mail address: gang_shao@zzu.edu.cn

Prof. Rui Zhang

Tel: +86-371-60632007

Fax: +86-371-60632600

E-mail address: zhangray@zzu.edu.cn

1.   M. Yu, C. Liang, M. Liu, X. Liu, K. Yuan, H. Cao and R. Che, *J. Mater. Chem. C*, 2014, **2**, 7275-7283.

2.   C. Liang, C. Liu, H. Wang, L. Wu, Z. Jiang, Y. Xu, B. Shen and Z. Wang, *J. Mater. Chem. A*, 2014, **2**, 16397-16402.

3.   Z. Yang, Z. Li, L. Yu, Y. Yang and Z. Xu, *J. Mater. Chem. C*, 2014, **2**, 7583-7588.

4.   A. Kumar, A. P. Singh, S. Kumari, P. K. Dutta, S. K. Dhawan and A. Dhar, *J. Mater. Chem. A*, 2014, **2**, 16632-16639.

5.   A. P. Singh, M. Mishra, P. Sambyal, B. K. Gupta, B. P. Singh, A. Chandra and S. K. Dhawan, *J. Mater. Chem. A*, 2014, **2**, 3581-3593.

6.   X. Sun, J. He, G. Li, J. Tang, T. Wang, Y. Guo and H. Xue, *J. Mater. Chem. C*, 2013, **1**, 765-777.

7.   L. Wang, Y. Huang, X. Sun, H. Huang, P. Liu, M. Zong and Y. Wang, *Nanoscale*, 2014, **6**, 3157-3164.

8.   C. He, S. Qiu, X. Wang, J. Liu, L. Luan, W. Liu, M. Itoh and K.-i. Machida, *J. Mater. Chem.*, 2012, **22**, 22160-22166.

9.   D. Sun, Q. Zou, Y. Wang, Y. Wang, W. Jiang and F. Li, *Nanoscale*, 2014, **6**, 6557-6562.

10.   J. Jiang, D. Li, D. Geng, J. An, J. He, W. Liu and Z. Zhang, *Nanoscale*, 2014, **6**, 3967-3971.

11.   G. Tong, Q. Hu, W. Wu, W. Li, H. Qian and Y. Liang, *J. Mater. Chem.*, 2012, **22**, 17494-17504.

12.   C. Gong, J. Zhang, X. Zhang, L. Yu, P. Zhang, Z. Wu and Z. Zhang, *J. Phys. Chem. C*, 2010, **114**, 10101-10107.

13.   B. Zhao, B. Fan, G. Shao, B. Wang, X. Pian, W. Li and R. Zhang, *Appl. Surf. Sci.*, 2014, **307**, 293-300.

14.   T. Liu, P. Zhou, J. Xie and L. Deng, *J. Appl. Phys.*, 2012, **111**, 093905.

15.   G. Wang, Z. Gao, S. Tang, C. Chen, F. Duan, S. Zhao, S. Lin, Y. Feng, L. Zhou and Y. Qin, *ACS Nano*, 2012, **6**, 11009-11017.

16.   G. Wang, Z. Gao, G. Wan, S. Lin, P. Yang and Y. Qin, *Nano Res.*, 2014, **7,** 704-716.

17.   Z. Wang, L. Wu, J. Zhou, B. Shen and Z. Jiang, *RSC Adv.*, 2013, **3**, 3309-3315.

18.   X. Liu, C. Feng, S. W. Or, Y. Sun, C. Jin, W. Li and Y. Lv, *RSC Adv.*, 2013, **3**, 14590-14594.

19.   X. L. Dong, X. F. Zhang, H. Huang and F. Zuo, *Appl. Phys. Lett.*, 2008, **92**, 013127

20.   X. F. Zhang, X. L. Dong, H. Huang, Y. Y. Liu, W. N. Wang, X. G. Zhu, B. Lv, J. P. Lei and C. G. Lee, *Appl. Phys. Lett.*, 2006, **89**, 053115.

21.   B. Wang, J. Zhang, T. Wang, L. Qiao and F. Li, *J. Alloys Compd.*, 2013, **567**, 21-25.

22.   X. Zhang, X. Dong, H. Huang, B. Lv, J. Lei and C. Choi, *J. Phys. D: Appl. Phys.*, 2007, **40**, 5383.

23.   C. Cui, Y. Du, T. Li, X. Zheng, X. Wang, X. Han and P. Xu, *J. Phys. Chem. B*, 2012, **116**, 9523-9531.

24.   Y.-J. Chen, G. Xiao, T.-S. Wang, Q.-Y. Ouyang, L.-H. Qi, Y. Ma, P. Gao, C.-L. Zhu, M.-S. Cao and H.-B. Jin, *J. Phys. Chem. C*, 2011, **115**, 13603-13608.

25.   C. Yan and D. Xue, *J. Phys. Chem. B*, 2006, **110**, 7102-7106..

26.   F. Gu, C. Z. Li, S. F. Wang and M. K. Lü, *Langmuir*, 2005, **22**, 1329-1332..

27.   B. Zhao, G. Shao, B. Fan, W. Zhao, Y. Xie and R. Zhang, *RSC Adv.*, 2014, **4**, 61219-61225.

28.   P. Zhang, X. Han, L. Kang, R. Qiang, W. Liu and Y. Du, *RSC Adv.*, 2013, **3**, 12694-12701.

29.   Y. Du, W. Liu, R. Qiang, Y. Wang, X. Han, J. Ma and P. Xu, *ACS Appl. Mater. Interfaces*, 2014, **6**, 12997-13006.

30.   B. Zhao, G. Shao, B. Fan, W. Li, X. Pian and R. Zhang, *Mater. Lett.*, 2014, **121**, 118-121.

31.   S. He, G.-S. Wang, C. Lu, J. Liu, B. Wen, H. Liu, L. Guo and M.-S. Cao, *J. Mater. Chem. A*, 2013, **1**, 4685-4692.

32.   B. Zhao, G. Shao, B. Fan, W. Zhao and R. Zhang, *RSC Adv.*, 2014, **4**, 57424-57429.

33. H. Li, Y. Huang, G. Sun, X. Yan, Y. Yang, J. Wang and Y. Zhang, *J. Phys. Chem. C*, 2010, **114**, 10088-10091..

34. X.-L. Shi, M.-S. Cao, J. Yuan, Q.-L. Zhao, Y.-Q. Kang, X.-Y. Fang and Y.-J. Chen, *Appl. Phys. Lett.*, 2008, **93**, 183118.

35. B. Zhao, G. Shao, B. Fan, C. Wang, Y. Xie and R. Zhang, *Powder Technol.*, 2015, **270**, 20-26..

36. X. Liu, J. Jiang, D. Geng, B. Li, Z. Han, W. Liu and Z. Zhang, *Appl. Phys. Lett.*, 2009, **94**, 053119.

37. X. Liu, D. Geng, H. Meng, P. Shang and Z. Zhang, *Appl. Phys. Lett.*, 2008, **92**, 173117.

38. P. Xu, X. Han, C. Wang, D. Zhou, Z. Lv, A. Wen, X. Wang and B. Zhang, *J. Phys. Chem. B*, 2008, **112**, 10443-10448.

39. G. Tong, J. Yuan, W. Wu, Q. Hu, H. Qian, L. Li and J. Shen, *CrystEngComm*, 2012, **14**, 2071-2079

40. T. Chen, F. Deng, J. Zhu, C. Chen, G. Sun, S. Ma and X. Yang, *J. Mater. Chem.*, 2012, **22**, 15190-15197..

41. P. Toneguzzo, O. Acher, G. Viau, F. Fiévet-Vincent and F. Fiévet, *J. Appl. Phys.*, 1997, **81**, 5546-5548

42. A. Aharoni, *J. Appl. Phys.*, 1991, **69**, 7762-7764..

43. P. F. Guan, X. F. Zhang and J. J. Guo, *Appl. Phys. Lett.*, 2012, **101**, 153108.

44. D. Chen, H. Quan, G. S. Wang and L. Guo, *ChemPlusChem*, 2013, **78**, 843-851.

45. H. Yu, T. Wang, B. Wen, M. Lu, Z. Xu, C. Zhu, Y. Chen, X. Xue, C. Sun and M. Cao, *J. Mater. Chem.*, 2012, **22**, 21679-21685.

46. M. Han, X. Yin, L. Kong, M. Li, W. Duan, L. Zhang and L. Cheng, *J. Mater. Chem. A*, 2014, **2**, 16403-16409

47. Y.-Z. Wei, G.-S. Wang, Y. Wu, Y.-H. Yue, J.-T. Wu, C. Lu and L. Guo, *J. Mater. Chem. A*, 2014, **2**, 5516-5524

48. B. Zhao, G. Shao, B. Fan, B. Sun, K. Guan and R. Zhang, *J. Mater. Sci.: Mater. Electron.,* 2014, **25**, 3614-3621.

49. P. H. Fang, *J. Chem. Phys. ,* 1965, **42**, 3411-3413.

50. S. He, C. Lu, G.-S. Wang, J.-W. Wang, H.-Y. Guo and L. Guo, *ChemPlusChem*, 2014, **79**, 569-576..

51. M. Wu, Y. D. Zhang, S. Hui, T. D. Xiao, S. Ge, W. A. Hines, J. I. Budnick and G. W. Taylor, *Appl. Phys. Lett.*, 2002, **80**, 4404-4406.

52. S. Xie, X.-N. Guo, G.-Q. Jin and X.-Y. Guo, *Phys. Chem. Chem. Phys.*, 2013, 15, 16104-16110..

53. J. Guo, X. Wang, P. Miao, X. Liao, W. Zhang and B. Shi, *J. Mater. Chem.*, 2012, **22**, 11933-11942.

54. J. Zhu, S. Wei, N. Haldolaarachchige, D. P. Young and Z. Guo, *J. Phys. Chem. C*, 2011, **115**, 15304-15310.

55. L.-S. Fu, J.-T. Jiang, C.-Y. Xu and L. Zhen, *CrystEngComm*, 2012, **14**, 6827-6832.

56. D. Micheli, C. Apollo, R. Pastore and M. Marchetti, *Compos. Sci. Technol.,* 2010, **70**, 400-409.

57. J. Xiang, J. Li, X. Zhang, Q. Ye, J. Xu and X. Shen, *J. Mater. Chem. A*, 2014, **2**, 16905-16914.

58. S. L. Wen, Y. Liu, X. C. Zhao, J. W. Cheng and H. Li, *Phys. Chem. Chem. Phys.*, 2014, **16**, 18333-18340

59. B. Lu, H. Huang, X. L. Dong, X. F. Zhang, J. P. Lei, J. P. Sun and C. Dong, *J. Appl. Phys.,* 2008, **104**, 114313.

60. R. Ji, C. Cao, Z. Chen, H. Zhai and J. Bai, *J. Mater. Chem. C*, 2014, **2**, 5944-5953.

61. B. Zhao, G. Shao, B. Fan, Y. Xie and R. Zhang, *J. Magn. Magn. Mater.*, 2014, 372, 195-200.

62. Z. H. Wang, L. W. Jiang, D. Li, J. J. Jiang, S. Ma, H. Wang, D. Y. Geng, J. An, J. He, W. Liu and Z. D. Zhang, *J. Appl. Phys*, 2014, **115**, 17A527.

63. P. Xu, X. Han, C. Wang, D. Zhou, Z. Lv, A. Wen, X. Wang and B. Zhang, *J. Phys. Chem. B*, 2008, **112**, 10443-10448.

64. B. Zhao, G. Shao, B. Fan, W. Zhao and R. Zhang, *Phys. Chem. Chem. Phys.*, 2015, **17**, 2531-2539.

RSC Advances Accepted Manuscript